VŠB – Technical University of Ostrava

University Study Programmes

Institute of Physics

Description of spin-polarized current in multilayer systems using Boltzmann transport equation

2014 Bc. Ondřej Stejskal

Supervisor: Mgr. Jaroslav Hamrle, PhD.

VŠB - Technical University of Ostrava
University Study Programmes
Institute of Physics

Diploma Thesis Assignment

Student: **Ondřej Stejskal**

Study Programme: N3942 Nanotechnology

Study Branch: 3942T001 Nanotechnology

Title: Popis spin-polarizovaného proudu v multivrstvách pomocí Botzmannovy transportní rovnice
Description of spin-polarized current using Boltzmann transport equation

Description:

Práce je zaměřena na popis elektronového transportu v multivrstevnatých strukturách pomocí Boltzmannovy transportní rovnice. Transport bude hlavně zaměřen na popis vodivosti a určení profilu proudové hustoty v multivrstvách se započtením vlivu reflexe a transmise elektronů na rozhraní. Tyto teoretické modely budou porovnány s experimentálními hodnotami vodivostí pro různé multivrstvy a dojde k určení reflexních a trasmisních koeficientů elektronů na rozhraních. Práce dále může zahrnovat zobecnění tohoto formalismu pro spin-polarizovaný a tepelný transport.

The thesis targets electron transport in multilayer structures using Boltzmann transport equation. The aim is to describe total conductivity and to determine profile of the charge current density in multilayers, including contribution of reflection and transmission coefficients on the interfaces. Those theoretical models will be compared with experimental conductivity determined for various multilayers, providing values of reflection and transmission coefficients on the interfaces. The thesis may further include generalization of this formalism for spin-polarized or thermal transport.

References:

[1] The mean free path of electrons in metals, E.H. Sondheimer, Advances in Physics 1, 1 (1952)
[2] Novel magnetoresistance effect in layered magnetic structures: Theory and experiment, J. Barnas, A. Fuss, R. E. Camley, P. Grunberg, W. Zinn, Phys. Rev. B 42, 8110 (1990).
[3] Boltzmann approach to dissipation produced by a spin-polarized current, A. A. Tulapurkar and Y. Suzuki, Phys. Rev. B 83, 012401 (2011).
[4] Current induced torques and interfacial spin-orbit coupling: Semiclassical modeling, Paul M. Haney, Hyun-Woo Lee, Kyung-Jin Lee, A. Manchon, and M. D. Stiles, Phys. Rev. B87, 174411 (2013).

Extent and terms of a thesis are specified in directions for its elaboration that are opened to the public on the web sites of the faculty.

Supervisor: **Mgr. Jaroslav Hamrle, Ph.D.**

Date of issue: 11.11.2013

Date of submission: 15.05.2014

prof. Dr. RNDr. Jiří Luňáček
Head of Department

VYSOKÁ ŠKOLA BÁŇSKÁ - TECHNICKÁ UNIVERZITA OSTRAVA
UNIVERZITNÍ STUDIJNÍ PROGRAMY

prof. Ing. Petr Noskievič, CSc.
Vice-rector for Study Affairs

Prohlašuji, že

- jsem byl seznámen s tím, že na moji diplomovou práci se plně vztahuje zákon č. 121/2000 Sb., autorský zákon, zejména § 35 - užití díla v rámci občanských a náboženských obřadů, v rámci školních představení a užití díla školního a § 60 - školní dílo.
- beru na vědomí, že Vysoká škola báňská - Technická univerzita Ostrava (dále jen „VŠB-TUO“) má právo nevýdělečně ke své vnitřní potřebě diplomovou práci užít (§ 35 ods. 3).
- souhlasím s tím, že diplomová práce bude v elektronické podobě uložena v Ústřední knihovně VŠB-TUO k nahlédnutí a jeden výtisk bude uložen u vedoucího diplomové práce. Souhlasím s tím, že údaje o kvalifikační práci budou zveřejněny v informačním systému VŠB-TUO.
- bylo sjednáno, že s VŠB-TUO, v případě zájmu z její strany, uzavřu licenční smlouvu s oprávněním užít dílo v rozsahu § 12 odst. 4 autorského zákona.
- bylo sjednáno, že užít své dílo - diplomovou práci nebo poskytnout licenci k jejímu využití mohu jen se souhlasem VŠB-TUO, která je oprávněna v takovém případě ode mne požadovat přiměřený příspěvek na úhradu nákladů, které byly VŠB-TUO na vytvoření díla vynaloženy (až do jejich skutečné výše).
- beru na vědomí, že odevzdáním své diplomové práce souhlasím se zveřejněním své práce podle zákona č. 111/1988 Sb., o vysokých školách a o změně a doplnění dalších zákonů (zákon o vysokých školách), ve znění pozdějších předpisů, bez ohledu na výsledek její obhajoby.

V Ostravě 15. května 2014 .....

Jméno a příjmení autora práce: Bc. Ondřej Stejskal

Adresa trvalého pobytu: Pustkovecká 367/25A, 708 00, Ostrava-Pustkovec

I declare I elaborated this thesis by myself. All literary sources and publications I have used are listed.

Ostrava, 15. května 2014 .....

I would like to thank to my family and friends for the support during my studies. I would also like to thank to my supervisor Jaroslav Hamrle for his helpfulness during my studies and for all the opportunities he has provided me. As far as this work is concerned, big thanks belong to André Thiaville for a great leadership and help, as large part of this work has been done during my summer stay in his laboratory in Orsay, Paris.

Abstrakt

Nedávné objevy spinového proudu, spinového Hallova efektu a Rashba efektu přitáhly nový zájem o transportní jevy v multivrstvách. Fuchs-Sondheimerova teorie, která je založena na Boltzmannově transportní rovnici, popisuje transpotní jevy v tenkých vrstvách. Ačkoli se jedná o článek vydaný roku 1952, teorie je stále používána a je v dobré shodě s experimenty. V této práci použijeme tuto teorii pro popis proudové hustoty v multivrstevnatém systém Ta/Pt/[Co/Ni]/Pt/Ta. Odpor multivrstvy je měřen pro různé tloušťky jednotlivých vrstev. Aplikováním Fuchs-Sondheimerova modelu získáme materiálové parametry vrstev a určíme rozložení proudu ve vzorku. Toto je pro multivrstvy velice důležité, protože spinové jevy, jako spinový Hallův jev a přenos spinového momentu, jsou úměrné proudové hustotě v blízkosti rozhraní feromagnetického materiálu.

Klíčová slova: Boltzmannova transportní rovnice, Fuchs-Sondheimerova teorie, spinový Hallův jev, přenos spinového momentu

Abstract

Recent discoveries of spin current, spin Hall effect and Rashba effect have attracted a new interest in transport phenomena in multilayer systems. The Fuchs-Sondheimer theory that is based on the Boltzmann transport equation covers the transport phenomena in thin films. Though the paper was released in 1952, the theory is still being used with great success and is in a great agreement with experiments. Within this work, we use this theory for the description of an in-plane current density in a multilayer system Ta/Pt/[Co/Ni]/Pt/Ta. The resistance of the multilayer is measured

as the function of the thicknesses of individual layers. Using the Fuchs-Sondheimer model we obtain the material parameters of the layers and the current distribution in the sample. This is of a great importance for multilayers, as the spin phenomena, like spin Hall effect and spin-transfer torque, are proportional to current densities in the vicinity of the interface with ferromagnetic material.

Keywords: Boltzmann transport equation, Fuchs-Sondheimer theory, spin Hall effect, spin-transfer torque

Contents

List of Figures

1 Introduction

Experiments by J.J. Thomson in 1897 led to the discovery of the electron as a particle with an elementary electric charge. This property causes an electron to interact with electromagnetic fields and enables to carry an electrical current. In 1922 the magnetic moment of the electron was discovered by Stern and Gerlach. Later, it was established that the intrinsic angular momentum of the electron, spin, is quantized, such that the projection of the momentum to the z-axis provides only two discrete values ($\pm\hbar/2$). Therefore, whenever a spin is measured in a given direction, it can be either spin-up or spin-down. The conventional electronics employs the charge of the electron as a carrier of information. However, the electron spin provides another degree of freedom to be handled and to be manipulated, for example by interaction with a magnetic field. This new field of physics is referred to as Spintronics [5, 6].

Probably the first observation of spin affecting electron transport dates back to 1857, when W. Thomson found that the resistance of a ferromagnetic metal depends on the angle between the magnetization and current direction (the anisotropic magnetoresistance (AMR) effect) [7]. Later on, other spin phenomena have been discovered, such as the giant magnetoresistance (GMR) [8, 9] and the tunneling magnetoresistance (TMR) [10]. Both effects has been successfully applied in the industry and GMR also earned itself a Nobel Prize in Physics in 2007. The GMR effect was initially discovered in a pillar spin valve sample, i.e. a non-ferromagnetic (N) metal sandwiched between two ferromagnets (F) [11]. The general requirement for spintronic devices is the ability to create, transport and detect spin currents. The creation of the spin current is generally called the spin injection and some ways of this creation have already been proposed and experimentally proved, e.g. by driving an electrical current from F material into N [12], spin pumping [13] or the spin Hall effect [14].

This thesis focuses on determining the current distribution in multilayer samples from the measurement of sample resistances. The current distribution is important for evaluating the spin Hall effect and spin-transfer torque.

In Chapter 2 the basics for the spin transport in ferromagnetic and non-ferromagnetic materials are introduced, including the spin Hall effect.

In Chapter 3 the Boltzmann transport equation is derived.

In Chapter 4 the Fuchs-Sondheimer model is introduced. We develop the formalism for multilayer sample and provide basic formulas.

In Chapter 5 we present the experimental results on series of multilayer samples. All the results can be seen in Appendix A.

The comparison of the theory with experiment is in Chapter 6. There we fit the measured data under various criteria and obtain parameters from which we then determine the current distribution.

2 Spin transport in metals

2.1 Ferromagnets

In general, magnetism originates from the magnetic moment of electrons, since the magnetic moment of nuclei is negligibly small. Electron has an orbital angular momentum due to its orbiting around its nucleus. Furthermore, it has its own intrinsic angular momentum called spin. Each electron can be considered as a small magnetic moment, but aligning many together results in a macroscopic magnetic field. In ferromagnetic materials the density of states (DOS) for spin-up and spin-down sub-bands is shifted by the exchange energy (Stoner model) as sketched in Fig.1 [6]. Hence, the number of spin-up and spin-down electrons is unequal.

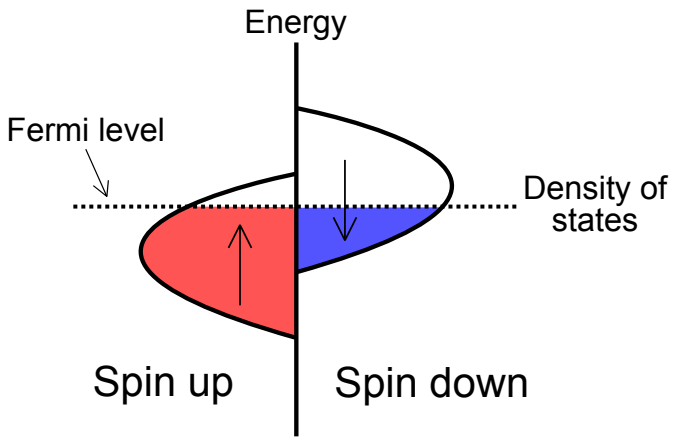

Figure 1: A schematic band structure for the Stoner model of ferromagnetism. An exchange interaction has split the energy of states with different spins. Hence, the states near the Fermi level are different for each spin direction. [1]

Due to the shift in the DOS, the ferromagnetic material is characterized by different bulk conductivities for the spin-up and spin-down electrons given by the Einstein relation:

$$\sigma_{\uparrow/\downarrow} = \frac{1}{3} e^2 N_{\uparrow/\downarrow} v_{F\uparrow/\downarrow} l_{e\uparrow/\downarrow} \tag{2.1}$$

where $\sigma_{\uparrow/\downarrow}$ are the spin-up and spin-down conductivities, e is the elementary charge, $N_{\uparrow/\downarrow}$ the DOS at the Fermi energy, $v_{F\uparrow/\downarrow}$ the average spin dependent Fermi velocity and $l_{e\uparrow/\downarrow}$ the average spin dependent electron mean free path. The current can be considered to consist of two separate spin channels (the two channel model) [15], where the sum corresponds to the charge current $I_{\mathrm{ch}} = I_{\uparrow} + I_{\downarrow}$ and the difference to the spin current $I_{\mathrm{sp}} = I_{\uparrow} - I_{\downarrow}$. The current flowing through a ferromagnet is in general spin-polarized. Thus it can affect the magnetization of the ferromagnet due to the spin-transfer torque, for example, inducing a domain wall motion [16].

2.2 Spin Hall effect

The spin Hall effect (SHE) is a spin-orbit coupling phenomenon that can be used to electrically generate or detect spin currents in non-magnetic systems [17]. It was predicted 40 years ago by Dyakonov and Perel [14]. They proposed that an unpolarized charge current causes a transverse spin current in systems with the spin-orbit coupling. The effect has a Hall symmetry, because the polarization axis of the spins is perpendicular to both the driving charge current and the transverse spin current.

The concepts for the experimental detection of the spin Hall effect were introduced almost 30 years later by Hirsch [18] and Zhang [19]. Hirsch proposed a device in which the spin current generated by SHE is injected into another part of the device, where it generates a charge current by the inverse SHE. This current can be measured electrically. Zhang suggested that the spin accumulation produced by the SHE can be detected by measuring an electrochemical potential using a ferromagnetic probe. However, the first measurements of the SHE were made using magneto-optical Kerr microscope [20] and p-n diodes [21].

When the spin current, generated in a non-magnet with the SHE, is injected into a ferromagnet, it affects its magnetization. This effect is described by the Slonczewski term [22] in the Landau-Lifshitz-Gilbert equation that describes the magnetization dynamics.

As mentioned above, in the case of the SHE, the electrons are preferentially scattered in different directions depending on their spin direction. In a non-magnetic material with positive SHE, the electrons are scattered in such direction that $(\mathbf{v}_\mathrm{i} \times \mathbf{v}_\mathrm{f}) \cdot \mathbf{S}$ is positive, where $\mathbf{v}_{\mathrm{i(f)}}$ is the electron velocity before (after) scattering and $\mathbf{S}$ is the electron spin direction. If we now have a ferromagnetic layer on top of a non-magnetic one (Fig. 2), the charge current, being in the $+x$ direction, injects the electrons with spin along $+y$ direction into the magnetic layer. The spin current causes a spin-transfer torque along the direction $-\mathbf{M} \times (\mathbf{M} \times \mathbf{m})$, where $\mathbf{M}$ is the magnetization of the ferromagnet and $\mathbf{m}$ is the direction of the magnetic moment of an electron and points along $-y$ direction since $\mathbf{m}$ and $\mathbf{S}$ are anti-parallel. This torque is often called the damping-like torque [2].

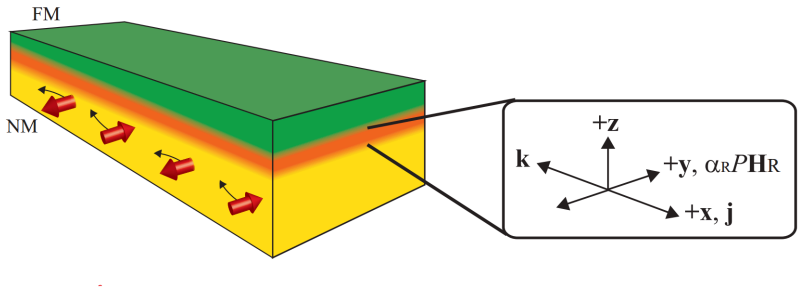

Figure 2: A schematic of a bilayer system. The current flowing through the non-magnetic layer induces a perpendicular spin current due to the spin Hall effect. The spin current enters the magnetic layer and affects the magnetization of the layer by the spin-transfer torque. [2]

Several experiments have been made involving these phenomena especially by Liu *et al.* [23], [24], [25]. [26]. In their experiments they quantify the magnitude of the spin Hall effect induced torque and they estimate the spin Hall angle of Pt to be about +0.076. They also demonstrate that this torque can switch the magnetization of the ferromagnet efficiently, making it a good candidate for magnetization controlling, e.g. the magnetic memory devices. They also estimate the spin Hall angle of

Ta to be -0.12 to -0.15, having an opposite sign compared to Pt, but being approximately two times larger. Recently, they have determined even larger spin Hall angle in W [27].

Other experiments that demonstrate the importance of the SHE in magnetization switching can be seen here [28], [29].

2.3 Multilayer sample

Having now a multilayer sample consisting of both ferromagnetic thin layers and layers with large SHE in an in-plane configuration (with an in-plane current), several phenomena occur. The general sample consists of a ferromagnetic material on top of a nonmagnetic material. An in-plane current in the magnetic material can induce domain wall motion (Fig. 3) due to the spin-transfer torque effect [30]. The current in non-magnet (with large SHE) injects a perpendicular-to-plane spin current to the magnetic layer which can also induce domain wall motion [16] or switch the magnetization of the ferromagnet [23], see Fig. 4. For these applications, it is important to know the current densities present in each layer of the sample, as these effects are proportional to them. Generally, the resistance of the whole multilayer is measured. Based on this information, we would like to determine the current distribution, which can be done using the Boltzmann approach.

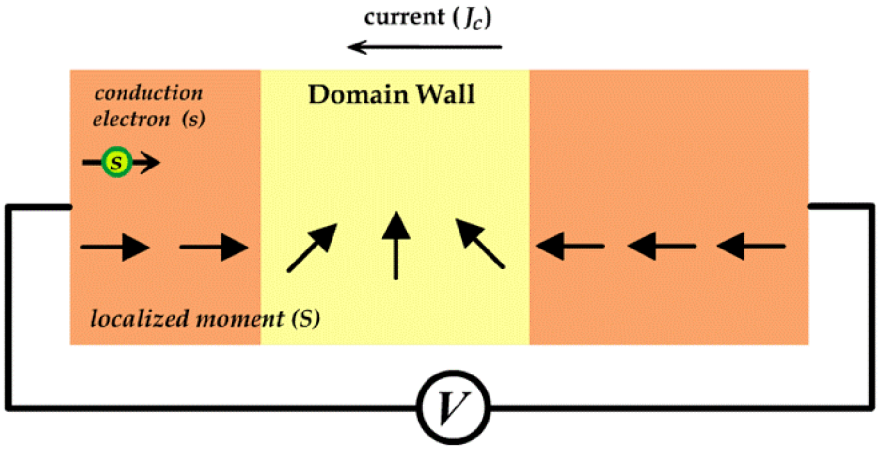

Figure 3: The charge current in the ferromagnetic layer induces the domain wall motion due to the spin-transfer torque. [3]

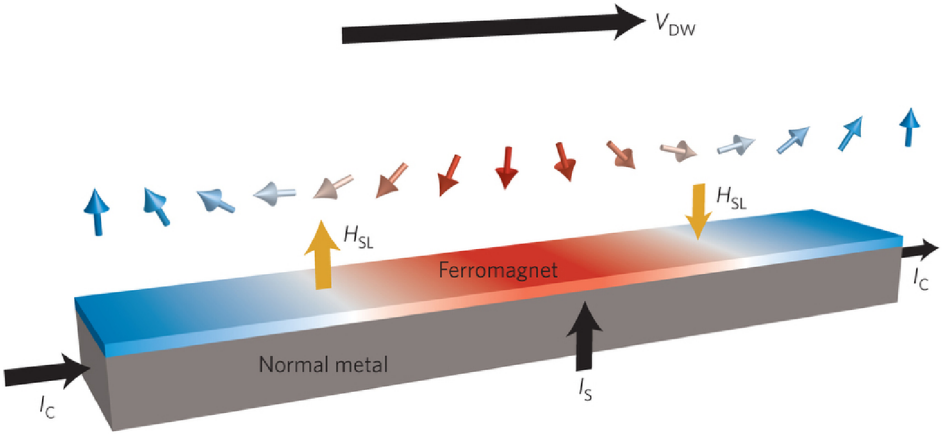

Figure 4: The charge current in non-metallic layer induces a transverse spin current due to the SHE. The spin-transfer torque affects the magnetization of the ferromagnet causing the domain wall motion. [4]

3 Boltzmann transport equation

For the description of transport phenomena in thin films, we use the Boltzmann transport theory. The transport properties of an electron gas are determined by the distribution function, the distribution of electrons in v-space (v meaning the velocity). Throughout this thesis we will always use v-space, though usually momentum space or k-space are being used. At equilibrium, the distribution function is the Fermi-Dirac function:

$$f_0(E) = \frac{1}{\exp\left(\frac{E-E_F}{k_B T}\right) + 1}, \tag{3.1}$$

E_F being the Fermi Energy, k_B Boltzmann constant and T temperature. This distribution function is independent of any present collisions as the collisions continuously remove electrons from one $\mathbf{v}$-state to another, keeping the net distribution the Fermi-Dirac function as long as there are no external influences. The Boltzmann transport equation describes the change of the distribution function in the presence of external forces. We denote $f(\mathbf{r}, \mathbf{v})$ the general distribution function of electrons, $f_0(\mathbf{v})$ being the equilibrium distribution function (Fermi-Dirac function). We need to determine how f changes with time. There are three possible reasons for the change in the electron distribution in v-space and r-space [31]:

1. Due to diffusion, electrons will move in and out of any volume element.
2. Due to the external forces, electrons will be changing their momentum (velocity) according to $m\,\mathrm{d}\mathbf{v}/\mathrm{d}t = \mathbf{F}_{\mathrm{ext}}$.
3. Due to the scattering processes, collisions.

In general, the Boltzmann transport equation can be written in the form:

$$\frac{\partial f}{\partial t} = \left(\frac{\partial f}{\partial t}\right)_{\mathrm{diff}} + \left(\frac{\partial f}{\partial t}\right)_{\mathrm{force}} + \left(\frac{\partial f}{\partial t}\right)_{\mathrm{coll}} \tag{3.2}$$

We will now calculate the partial time derivatives of the distribution function due to each source.

3.1 Diffusion

In a time interval δt, the electron moves a distance $\mathbf{v}\delta t$, $\mathbf{v}$ being the velocity of an electron. Thus the number of electrons in the neighborhood of $\mathbf{r}$ at time $t = \delta t$ equals to the number of electrons in the neighborhood of $\mathbf{r} - \mathbf{v}\delta t$ at time $t = 0$. Therefore [31]:

$$f(\mathbf{r}, \delta t) = f(\mathbf{r} - \mathbf{v}\delta t, 0) \tag{3.3}$$

$$f(\mathbf{r}, 0) + \frac{\partial f}{\partial t}\delta t = f(\mathbf{r}, 0) - \frac{\partial f}{\partial \mathbf{r}} \cdot \mathbf{v}\delta t \tag{3.4}$$

$$\left(\frac{\partial f}{\partial t}\right)_{\text{diff}} = -\mathbf{v} \cdot \nabla_{\mathbf{r}} f \tag{3.5}$$

3.2 External forces

The velocity $\mathbf{v}$ of an electron evolves under the action of external forces according to Newton's equation of motion. In the presence of an electric ($\mathbf{E}$) and magnetic ($\mathbf{B}$) field the change of $\mathbf{v}$ is given by:

$$\frac{\mathrm{d}\mathbf{v}}{\mathrm{d}t} = \frac{\mathbf{F}_{\text{ext}}}{m} = -\frac{e}{m}(\mathbf{E} + \mathbf{v} \times \mathbf{B}) \tag{3.6}$$

As mentioned above, e is the elementary charge and by definition $e > 0$.

In analogy to the diffusion term, the electrons at time $t = 0$ with velocity $\mathbf{v} - \mathrm{d}\mathbf{v}/\mathrm{d}t\ \delta t$ will have velocity $\mathbf{v}$ at time $t = \delta t$ [31]:

$$f(\mathbf{v}, \delta t) = f(\mathbf{v} - \mathrm{d}\mathbf{v}/\mathrm{d}t\ \delta t, 0) \tag{3.7}$$

$$f(\mathbf{v}, 0) + \frac{\partial f}{\partial t}\delta t = f(\mathbf{v}, 0) - \frac{\partial f}{\partial \mathbf{v}} \cdot \frac{\partial \mathbf{v}}{\partial t}\delta t \tag{3.8}$$

$$\left(\frac{\partial f}{\partial t}\right)_{\text{force}} = -\frac{\partial \mathbf{v}}{\partial t} \cdot \nabla_{\mathbf{v}} f = \frac{e}{m}(\mathbf{E} + \mathbf{v} \times \mathbf{B}) \cdot \nabla_{\mathbf{v}} f \tag{3.9}$$

Substituting the two terms (3.5, 3.9) to the Boltzmann transport equation (3.2) and rearranging, we get:

$$\frac{\partial f}{\partial t} + \mathbf{v} \cdot \nabla_{\mathbf{r}} f + \frac{\partial \mathbf{v}}{\partial t} \cdot \nabla_{\mathbf{v}} f = \left(\frac{\partial f}{\partial t}\right)_{\text{coll}} \tag{3.10}$$

3.3 Collisions

The collision term is in general very complicated and takes the form of scattering integrals (Fermi golden rule in quantum mechanics). Usually, it has to be solved numerically. For simplicity we use the relaxation time approximation [32]:

$$\left(\frac{\partial f}{\partial t}\right)_{\text{coll}} = -\frac{f - f_0}{\tau} \tag{3.11}$$

with τ being the relaxation time. The relaxation time need not to be a constant and may depend, for example, on velocity. If v is the mean velocity of those electrons to which τ refers, then the corresponding mean free path λ is defined by $\lambda = v\tau$. The detailed theory of the conductivity in metals shows that such a mean free path does exist under certain conditions for quasi-free conduction electrons, so that it can always be defined for scattering by impurity atoms and by lattice vibrations above the Debye temperature. So for the electrical conductivity phenomena, it is a reasonable approximation [32].

The meaning of the collision term as defined above (Eq. 3.11) can be simply understood by the following example. Assume a slightly perturbed system (in non-equilibrium) with spatial uniformity and no external forces. This can be done for example, by putting a spatially uniform sample into the electric field and then turning the field off. Such a system is at time $t = 0$ (turning the field off) in a state that is described by non-equilibrium distribution function f. The diffusion term and force term disappear (because of the spatial uniformity and no external field present) and the Boltzmann equation simplifies to:

$$\frac{\partial f}{\partial t} = -\frac{f - f_0}{\tau} = -\frac{\delta f}{\tau} \tag{3.12}$$

which can be easily solved. We use δf to denote the difference $f - f_0$, meaning how the actual distribution of the system differs from the equilibrium distribution. The solution of this differential equation is:

$$\delta f(t) = \delta f(0) \exp\left(-\frac{t}{\tau}\right) \tag{3.13}$$

The distribution function goes exponentially to the equilibrium, with rate given by τ.

By putting it all together, we get the Boltzmann transport equation in the form:

$$\frac{\partial f}{\partial t} + \mathbf{v} \cdot \nabla_{\mathbf{r}} f + \frac{\partial \mathbf{v}}{\partial t} \cdot \nabla_{\mathbf{v}} f = -\frac{f - f_0}{\tau} \tag{3.14}$$

The Boltzmann equation in this form will be used in the following Chapter.

4 Fuchs-Sondheimer model

Our description of the electron transport in multilayers is based on the semi-classical Fuchs-Sondheimer model [32], since the thicknesses of individual layers will be smaller than the electron mean free path. We start with a single thin film and then apply the mechanism on a multilayer sample.

4.1 Thin film

Consider a thin metal film of a given thickness a surrounded by non-conducting material. The z-axis is perpendicular to plane, the surface being the planes $z = 0$ and $z = a$. The problem is essentially one-dimensional one and the distribution function for electrons $f(z, \mathbf{v})$ can be written in the form [32]:

$$f(z, \mathbf{v}) = f_0(\mathbf{v}) + g(z, \mathbf{v}) \tag{4.1}$$

where $f_0(\mathbf{v})$ is the equilibrium distribution function and $g(z, \mathbf{v})$ depends on space only through z. The electric field E is supposed to be in the x-direction, so the Boltzmann equation (3.14) reduces to:

$$\frac{\partial g}{\partial z} + \frac{g}{\tau v_z} = \frac{eE}{m v_z} \frac{\partial f_0}{\partial v_x} \tag{4.2}$$

where e ($e > 0$) and m are the electron charge and effective mass, τ is the relaxation time, v_x and v_z the components of the velocity vector in x and z directions respectively.

Note that we consider a steady state, so the distribution function f is not explicit function of time, $\partial f/\partial t = 0$. We assume no magnetic field is applied. The general solution of the Boltzmann equation (Eq. 4.2) $g_{\pm}(z, \mathbf{v})$ (g_+ corresponding to the electrons moving in the positive z direction, g_- to the electrons moving in the negative z direction) can be written in the form [32]:

$$g_{\pm}(z, \mathbf{v}) = \frac{eE\tau}{m} \frac{\partial f_0(\mathbf{v})}{\partial v_x} \left[1 + F_{\pm}(\mathbf{v}) \exp\left(\frac{\mp z}{\tau |v_z|} \right) \right] \tag{4.3}$$

where $F_{\pm}(\mathbf{v})$ are arbitrary functions to be determined from the boundary conditions.

To determine $F_{\pm}(\mathbf{v})$ we have to introduce the boundary conditions at the surface of the film (called Fuchs boundary conditions). We assume that a fraction p of the electrons is scattered elastically at the surface with reversal of the velocity component v_z. The rest $(1-p)$ is scattered diffusively, completely losing their drift velocity. p is supposed to be a constant independent of the direction of motion of the electrons. Then the boundary conditions can be written down:

$$g_+ = pg_-, \qquad \text{at } z = 0 \tag{4.4}$$

$$1 + F_+ = p(1 + F_-), \qquad \text{at } z = 0 \tag{4.5}$$

$$g_- = pg_+, \qquad \text{at } z = a \tag{4.6}$$

$$1 + F_- \exp\left(\frac{a}{\tau|v_z|}\right) = p\left(1 + F_+ \exp\left(-\frac{a}{\tau|v_z|}\right)\right), \qquad \text{at } z = a \tag{4.7}$$

We solve for $F_{\pm}(\mathbf{v})$ to get:

$$F_+ = -\frac{1-p}{1-p\exp\left(-\frac{a}{\tau|v_z|}\right)} \tag{4.8}$$

$$F_- = -\frac{1-p}{1-p\exp\left(-\frac{a}{\tau|v_z|}\right)} \exp\left(-\frac{a}{\tau|v_z|}\right) \tag{4.9}$$

If we assume only elastic scattering ($p = 1$), both $F_{\pm}(\mathbf{v})$ end up being 0 and the distribution functions $g_{\pm}$ are no longer functions of z. Indeed, elastic scattering means no loss of the drift velocity at the surfaces, so the thin film behaves as a bulk with no boundaries at all.

We can calculate the current density by [32]:

$$J(z) = -e \int v_x g \mathrm{d}\mathbf{v} \tag{4.10}$$

which can not be solved analytically in general. For comparison with experiment, we require the conductivity of the film, so we must average the current density over all values of z from 0 to a to obtain [32]:

$$\sigma = \frac{1}{Ea} \int_0^a J(z) dz \tag{4.11}$$

These integrals can be evaluated analytically only in limiting cases for thick film and very thin film. Here we present only the results [32]. In both cases $p = 0$ and for thick film ($a \gg \lambda$), λ being the electron mean free path, we get:

$$\frac{\sigma_0}{\sigma} = 1 + \frac{3\lambda}{8a} \tag{4.12}$$

For very thin film ($a \ll \lambda$):

$$\frac{\sigma_0}{\sigma} = \frac{4\lambda}{3a \ln\left(\frac{\lambda}{a}\right)} \tag{4.13}$$

σ_0 is the bulk conductivity, given from Drude model by:

$$\sigma_0 = \frac{ne^2\tau}{m} \tag{4.14}$$

where n is the density of electrons.

4.2 Multilayer

We can now apply the single thin film results for a multilayer sample. The distribution function in each layer is governed by the Boltzmann transport equation in the form of Eq. (4.2), which has the solution (4.3). So we need to determine $F_{\pm}(\mathbf{v})$ from the boundary conditions. We will use the formalism described by Barnas et al. [33]. For simplicity, we treat the electron transport as spin independent. First, we apply the Fuchs boundary conditions at the bottom and top interfaces (of the whole multilayer) using coefficients p_{bot} and p_{top} corresponding to the Fuchs specularity factors. Furthermore, inner interfaces are created.

Assume an interface between two materials A (with parameters τ_{A} and m_{A}) and B (τ_{B}, m_{B}). We introduce coefficients of specular transmission T and reflection R ($1 - R - T$ corresponding to diffusive scattering) and for simplicity we neglect any angular dependence of these coefficients (like for the Fuchs boundary conditions). The boundary conditions for such interface can be written down:

$$g_{\mathrm{B}+} = Rg_{\mathrm{B}-} + Tg_{\mathrm{A}+} \tag{4.15}$$

$$g_{\mathrm{A}-} = Rg_{\mathrm{A}+} + Tg_{\mathrm{B}-} \tag{4.16}$$

If we now plug in the solution for g (Eq. 4.3) for both materials (A,B), the relaxation times (τ) and effective masses (m) do not cancel out as in the previous case, because now we have distribution functions of different materials on each side of the equations. This difference in electronic properties of two adjacent materials will be taken into account by the parameter y (in correspondence with [33]), $y_{\mathrm{AB}} = \frac{m_{\mathrm{A}}\tau_{\mathrm{B}}}{m_{\mathrm{B}}\tau_{\mathrm{A}}}$. In our calculations we set $y_{\mathrm{AB}} = \sigma_{0\mathrm{B}}/\sigma_{0\mathrm{A}}$, where $\sigma_{0\mathrm{A}}$ ($\sigma_{0\mathrm{B}}$) is the bulk conductivity of material A (B). This choice will be discussed in more detail in Appendix A (sec. 8).

The coefficients of specular transmission T and reflection R will, in general, differ for each interface. By applying these boundary conditions, we get a set of $2N$ equations of $2N$ variables, where N is the number of layers in the sample (for every layer we have $F_{\pm}$). These equations are the spin independent version of the ones shown in [33]. We introduce β, the angle between the z axis and the velocity vector $\mathbf{v}$, and $\lambda = v_F\tau$, which is the electron mean free path, v_F being the Fermi velocity. These definitions enable us to consider the $F_{\pm}$ as functions of β. Note that all mentioned parameters ($F_{\pm}(\beta), \lambda, v_F, \tau$) will be in general different for each layer. These equations (to determine $F_{\pm}(\beta)$) will be solved only numerically. An example of how the boundary conditions for two layers look like in a matrix form can be found in Appendix B (sec. 9).

Once we have $F_{\pm}(\beta)$, we plug them in to Eq. 4.3 to get the distribution functions of each layer. Using Eqs. 4.10 and 4.11 we get the final formula for the total conductivity of a multilayer sample:

$$\begin{aligned}\sigma_{\mathrm{tot}} = \frac{1}{d}\int \mathrm{d}z \int_0^{\pi/2} \frac{3}{4}\sigma_0(z)\sin^3\beta \\ \times \left[2 + F_+(\beta, z)\exp\left(-\frac{z}{\lambda(z)\cos\beta}\right) + F_-(\beta, z)\exp\left(\frac{z}{\lambda(z)\cos\beta}\right)\right]\mathrm{d}\beta\end{aligned} \tag{4.17}$$

where d is the total thickness of the multilayer and σ_0 the bulk conductivity. The dependence of σ_0, λ and $F_{\pm}$ on z simply means that they differ for each layer (in given layer, they do not vary with z). The integration over z can be easily figured out analytically, but the integration over β is performed numerically (in more detail in sec. 6). Finally, we multiply the total conductivity of the sample by the total thick-

ness to get the sheet conductance, $G_{\mathrm{tot}} = \sigma_{\mathrm{tot}} d$, which we will use for the comparison with measured results.

We will be also interested in the current distribution in the sample, from Eq. 4.10 we get:

$$\begin{aligned} \frac{J(z)}{E} &= \sigma_0(z) + \frac{3}{4}\sigma_0(z) \int_0^{\pi/2} \sin^3\beta \\ &\quad \times \left[F_+(\beta, z) \exp\left(-\frac{z}{\lambda(z)\cos\beta} \right) + F_-(\beta, z) \exp\left(\frac{z}{\lambda(z)\cos\beta} \right) \right] \mathrm{d}\beta \end{aligned} \tag{4.18}$$

where the dependence of σ_0, λ and $F_\pm$ on z has the same meaning as in the previous case. On the other hand, the current density $J(z)$ will be function of z even in a given layer, because compared to Eq. 4.17, we have removed the integration over z and the exponentials do depend explicitly on z.

5 Experimental results

The samples were fabricated and investigated by Shunsuke Fukami, Center for Spintronics Integrated Systems, Tohoku University, Sendai, Japan. The nominal sample is shown in Fig. 5 and has the structure (sub/Ta(3)/Pt(1.6)/[Co(0.3)/Ni(0.6)] 4.5/Pt(1.6)/Ta(3)), where the numbers in brackets are the thicknesses in nanometers, and 4.5 is the number of Co/Ni stacks. In total, five series were fabricated: varying the bottom Ta (TaUL) thickness (Fig. 6a), bottom Pt (PtUL) thickness (Fig. 6b), Co/Ni stacking number (Fig. 6c), top Pt (Ptcap) thickness (Fig. 6d) and top Ta (Tacap) thickness (Fig. 6e). For each sample, the sheet resistance (for the current in plane setup) was measured five times and their average was computed. The whole list of measured sheet resistances is shown in Appendix A (sec. 8).

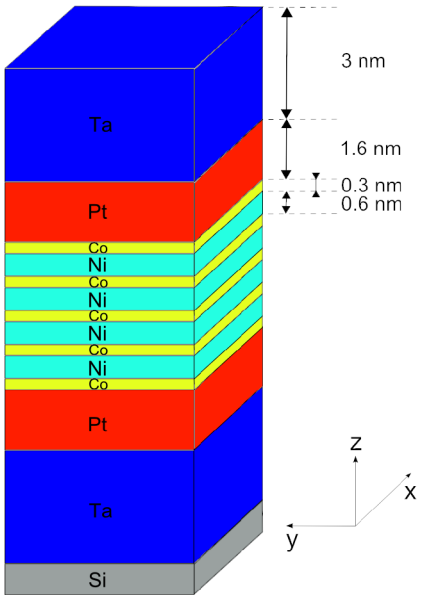

Figure 5: The nominal sample with the thicknesses of individual layers. In the bottom right corner, there is the definition of coordinates. Current flows in the x-direction.

The Ta thickness (for both top and bottom) is varied from 1 nm to 5 nm with step 1 nm, the Pt thickness (top and bottom) is varied from 0.4 nm to 4 nm with step 0.4 nm and the Co/Ni stacking number from 1 (one layer of Co and one layer of Ni) to 6.5 (six Co layers and five Ni layers). Note, that each series contains the nominal sample (sub/Ta(3)/Pt(1.6)/[Co(0.3)/Ni(0.6)]4.5/Pt(1.6)/Ta(3)), thus this sample was made five times. As can be seen in Appendix A (sec. 8), these five measured values are scattered in some degree, which reflects the performance limitations of the sample fabrication.

To be able to perfectly fit the measured results, we will set all five nominal samples to a single value (discussed in more detail in Appendix C, sec. 10). Thus we compute their average and correct all the measured values in such a way, that all the nominal samples have the same value of the sheet resistance. It means that the sheet resistances of all samples in each series are multiplied by the same coefficient (but different for every series) such that the nominal sample has its value of the sheet resistance equal to the computed average. This correction would correspond to a slight change in the deposition rate of the sputtering machine between the series, causing all the thicknesses to be smaller or larger by the same factor. Another possibility would be to offset all values within each series by the same amount. Both ways of correcting the values differ negligibly.

The original values of the sheet resistances are shown in Fig. 6. The term sheet resistance is used for the current in plane setup. Common unit for sheet resistance is Ω/sq., which is dimensionally equal to Ω, but is used to avoid the misinterpretation with the bulk resistance. We will be fitting the sheet conductances ($G = 1/R$) shown in Fig. 7. Note that the correct units for sheet conductances are mS·squares, but we will use just mS for simplicity. The conductances are additive (in the case of independent layers) and their behaviour is more intuitive, therefore we have decided to work with them. The exact numerical values (rounded to 1 decimal place) are shown in Appendix A (sec. 8). Note that, for each series, the evolution of resistance with thickness is smooth, with a clear trend, indicating a very good reproducibility

of the sample fabrication. Between the series, a small variation of resistance for the nominal sample occurs (especially when varying the Ta thicknesses).

Our model is based on the Fuchs-Sondheimer model (see sec. 4) and our goal is to reproduce all the measured results with a single set of thickness independent parameters. Using the same model, we will be interested in the distribution of current (important for the spin Hall effect in Pt).

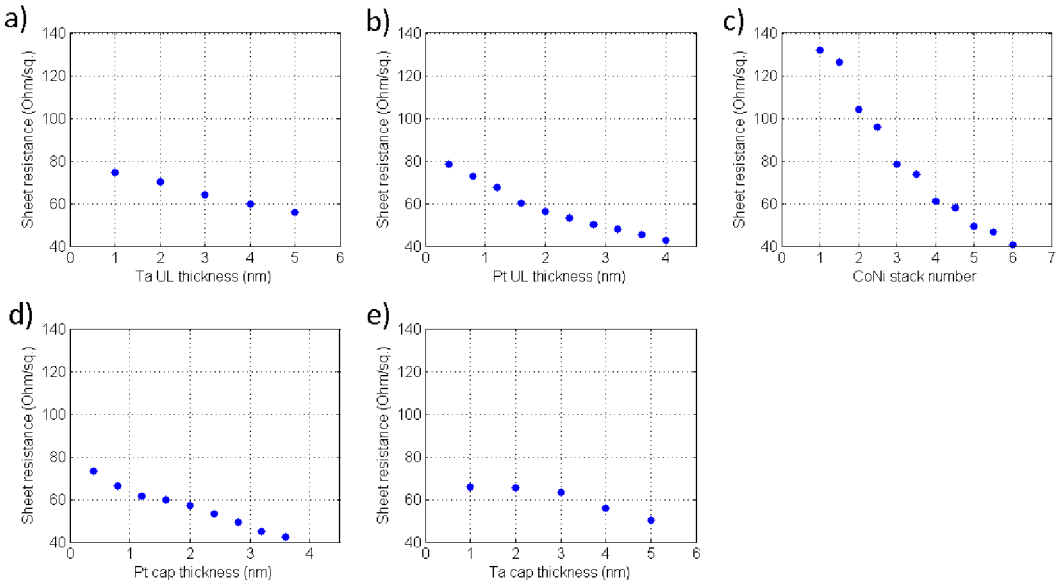

Figure 6: Experimental values of sheet resistances for all samples. The staircase shape of the Co/Ni stack number dependence shows that Co and Ni layers differ.

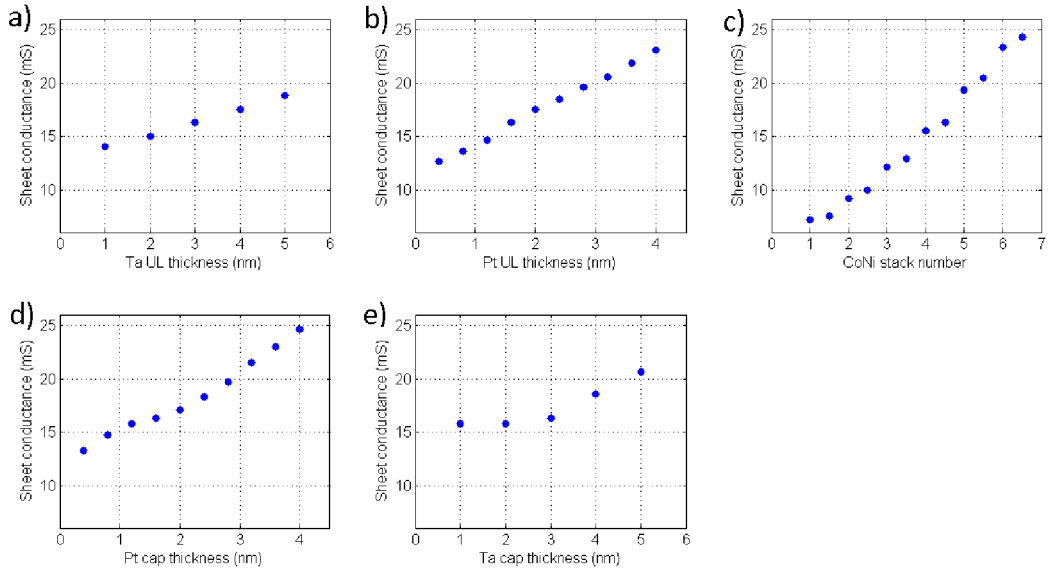

Figure 7: Corrected experimental values of sheet conductances for all samples

6 Fitting experimental results

For simplicity, the electron transport will be considered as spin independent, therefore all the layers will be treated as non-ferromagnetic (we assume that in Co and Ni, all the current is carried by one-type-of-spin electrons, thus we can treat them as spin independent). This enables us to reduce the number of parameters entering the model. Each layer is described by its bulk resistivity ρ_0 (or conductivity σ_0, which are in reciprocal relation $\rho_0 = 1/\sigma_0$) and the mean free path λ, both thickness independent. We will treat top and bottom Ta as well as top and bottom Pt separately, since their quality will be generally different (bottom Ta grows on a Si substrate, top Ta on top Pt; similar argument holds for both Pt layers). On the other hand, for simplicity, we treat all the Co (and also Ni) layers as having the same bulk parameters, though in reality they may differ.

The outer interfaces are characterized by the Fuchs specularity coefficients and the inner interfaces by specular transmission and reflection coefficients. For integer number of Co/Ni stacks, an interface Ni/Ptcap is created, but we will keep the coefficients as if it was Co/Ptcap interface (but parameter y will change), since Co and Ni are similar materials (neighbors in the periodic table).

Thus the total number of parameters is 24 (see Fig. 8), but it will be further reduced later. In our fitting, we are looking for the minimum of the sum of the squares of differences of computed and measured values (called error in following). To be able to compare among different optimizations, we present also root mean square errors (RMS). The integration over β (Eq. 4.17) is performed by rectangle method.

To reproduce the thickness dependences (Fig. 7a, b, d, e), only the thickness of particular layer will change, keeping the others fixed on their nominal values (as shown in Fig. 5), also keeping the number of layers. To reproduce the dependence of the conductance of the sample on the Co/Ni stack number (Fig. 7c), the total number of layers will be changing, since we have decided to treat Co and Ni as separate layers, but the thicknesses of all layers will stay on their nominal values.

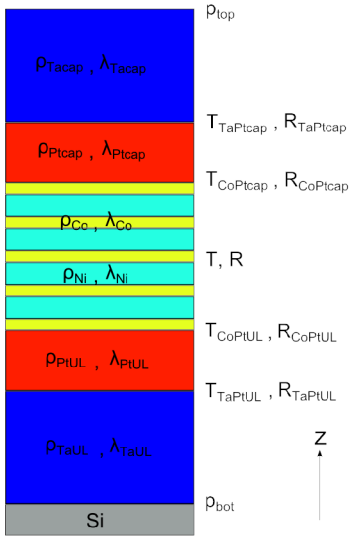

Figure 8: The nominal sample with all unknown parameters. Each layer is described by bulk conductivity σ_0 and electron mean free path λ, thus by 12 parameters in total. Each interface is described by specular reflection R and specular transmission T coefficients, except the bottom and top interface, where only reflection can occur.

First important result is that there is no way to fit all the data with a single set of thickness independent parameters (physically plausible) within reasonable error. But that is not suprising as we expect strong thickness dependence of Ta parameters (which may be caused by the presence of the β-Ta phase for low thicknesses [34]). So we confine ourselves only to Pt thickness dependences and Co/Ni stacking number dependence. Both Ta layers thicknesses will stay on their nominal values.

6.1 Pt-CoNi-Pt model

In this section, we will be fitting PtUL, Co/Ni and Ptcap dependences. Leaving the resistivities and mean free paths unconstrained (without upper boundaries), one obtains almost perfect fit (Fig. 9). The parameters are listed in Tab. 1. The values of

resistivities and mean free paths are (and always will be) rounded to 1 decimal place and the values of transmission coefficients to 2 decimal places. All reflection coefficients are zero (and are zero in any case, which is expectable for metallic samples). The corresponding current profile of the nominal sample with obtained parameters is shown in Fig. 10. We will always present only the current profile of the nominal sample. The numbers with % correspond to the percentage of the total current flowing through a given layer (for Co/Ni multilayer we present only the percentage of the current through the whole multilayer).

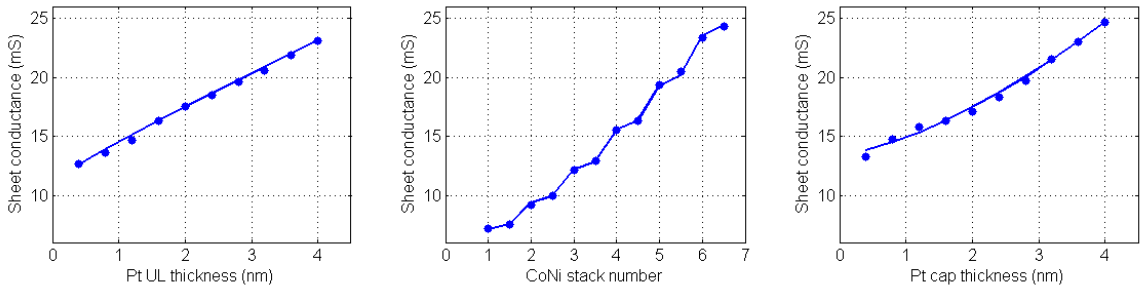

Figure 9: The result of the unconstrained Pt-CoNi-Pt model. The points correspond to the experimental values of sheet conductance as functions of PtUL and Ptcap thicknesses and CoNi stack number. The solid line is the result of the unconstrained fit.

The perfect fit is obtained for the cost of meaningfulness of the parameters. The high resistivity and mean free path of Ta layers can be justified by the fact that we are not fitting Ta thickness dependences, thus their values do not play an important role in other dependences. Changing the values of Ta simply shifts all the conductances equally. The high values of Co and Ni mean free paths can also be intuitively understood from the current profile (Fig. 10). The whole Co/Ni layer has its current profile similar to the one for a single layer, thus we can think that there is some mixing between Co and Ni. Bottom Pt layer has its bulk values reasonable, but top Pt has unrealistically high mean free path and we cannot think of any justification for this. Another intriguing fact is that there is more current flowing through the

Table 1: Obtained parameters for unconstrained Pt-CoNi-Pt model

	ρ_0 ($\mu\Omega$ cm)	λ (nm)		Error (mS^2)	1.53
TaUL	843.5	93.5		RMS (mS)	0.22
PtUL	35.7	2.2		T	1.00
Co	26.8	88.8		T_{TaPtUL}	0.12
Ni	6.6	49.3		T_{CoPtUL}	0.58
Ptcap	8.6	44.3		T_{CoPtcap}	0.13
Tacap	837.0	100.0		T_{TaPtcap}	0.17

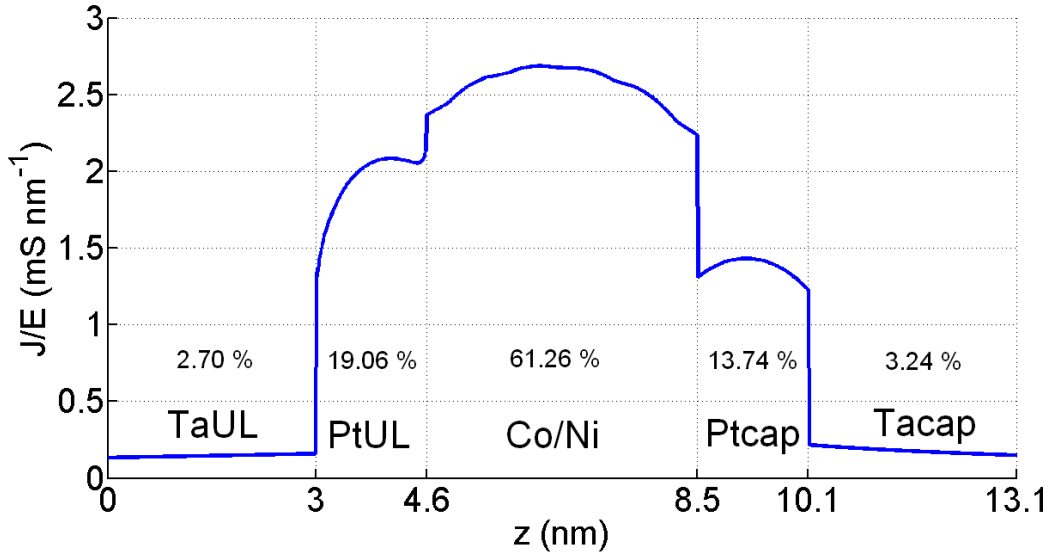

Figure 10: Current profile for unconstrained Pt-CoNi-Pt model

bottom Pt than through the top Pt, but we would expect the opposite, based on our previous knowledge of the sample.

Now we will make the same fit but putting some constraints on the upper boundaries. Namely, we will limit the mean free path to be less than 10 nm and also Ta resistivities to be under 300 $\mu\Omega$ cm. As result, we present the fit (Fig. 11), parameters

Table 2: Obtained parameters for constrained Pt-CoNi-Pt model

	ρ_0 ($\mu\Omega$ cm)	λ (nm)		Error (mS^2)	4.02
TaUL	300.0	10.0		RMS (mS)	0.35
PtUL	29.0	8.2		T	1.00
Co	50.0	10.0		T_{TaPtUL}	0.00
Ni	14.6	10.0		T_{CoPtUL}	0.66
Ptcap	17.6	10.0		T_{CoPtcap}	0.00
Tacap	300.0	10.0		T_{TaPtcap}	0.00

(Tab. 2) and the current distribution (Fig. 12) for the comparison with the previous case.

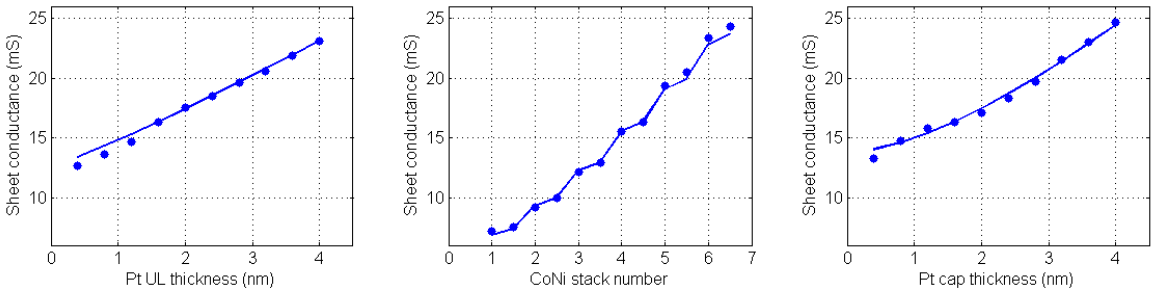

Figure 11: All the dependences obtained by constrained Pt-CoNi-Pt model.

The error increases approximately by a factor of 3, but the parameters now have slightly more reasonable values, though they mostly reach the upper constraint. Comparing the dependences (Fig. 9 with Fig. 11), one can see just small changes in the bottom Pt dependence (for small thicknesses) and the Co/Ni stacking number dependence. From this fact we can already conclude, that there is probably some mixing between Co and Ni as mentioned above, which forms a new single layer (also in the current profile (Fig. 12) we can see that now they do not act as a single layer). Again there is more current flowing through the bottom Pt (compared to top

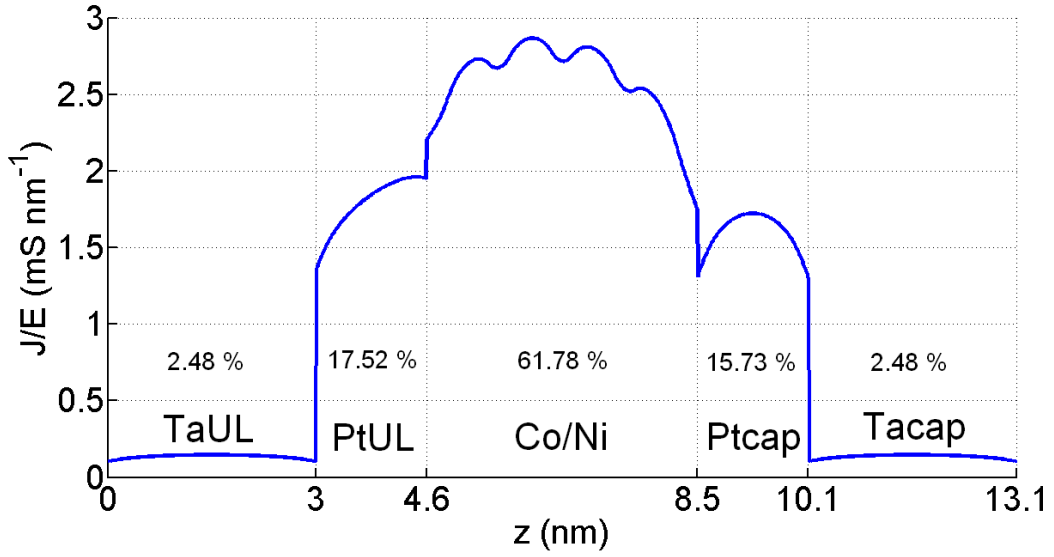

Figure 12: Current profile for constrained Pt-CoNi-Pt model

Pt), now caused by high transmission coefficient between bottom Pt and Co. This inversed current seems to be a general feature of this fitting. Even if we force the transmission coefficients to be symmetrical (i.e. $T_{\mathrm{CoPtUL}} = T_{\mathrm{CoPtcap}}$), both will end up being equal to zero, but the mean free path of the bottom Pt will be lowered, resulting again in more current in the bottom Pt.

To avoid the inversed current distribution, we must admit a thickness dependence of parameters for bottom Pt.

6.2 CoNi-Pt model

In this model, we fit only Co/Ni and Ptcap dependences. Excluding the PtUL thickness dependence from the fitting enables to further decrease the number of parameters and still being able to obtain good result. Moreover, we introduce the bulk constraint for Pt layers. From the Drude model the conductivity and the mean free

path for a bulk material are:

$$\sigma_0 = \frac{ne^2\tau}{m} \tag{6.1}$$

$$\lambda = v_F\tau \tag{6.2}$$

Then:

$$\rho_0\lambda = \frac{\lambda}{\sigma_0} = \frac{mv_F}{ne^2} \tag{6.3}$$

which does not contain the relaxation time τ. In [35] the bulk conductivity and mean free path were obtained for several Pt samples. Depending on the quality of the layer, the product $\rho_0\lambda$ lies between 200 and 400 $\mu\Omega$·cm·nm. So we will keep the product for the top Pt on the lowest value (200), since we think it should be a high quality layer. On the other hand, for the bottom Pt we will add a new fitting constraint, namely the product will be limited to 400 as an upper boundary. The mean free path for top Pt is forced to be less than 10 nm (that is the only boundary that is reached during the optimization). The results are shown in Fig. 13, Tab. 3 and Fig. 14. Note that the error is now incomparable with the ones in previous section, as we have removed PtUL thickness dependence, but the RMS has approximately the same value as in the unconstrained case.

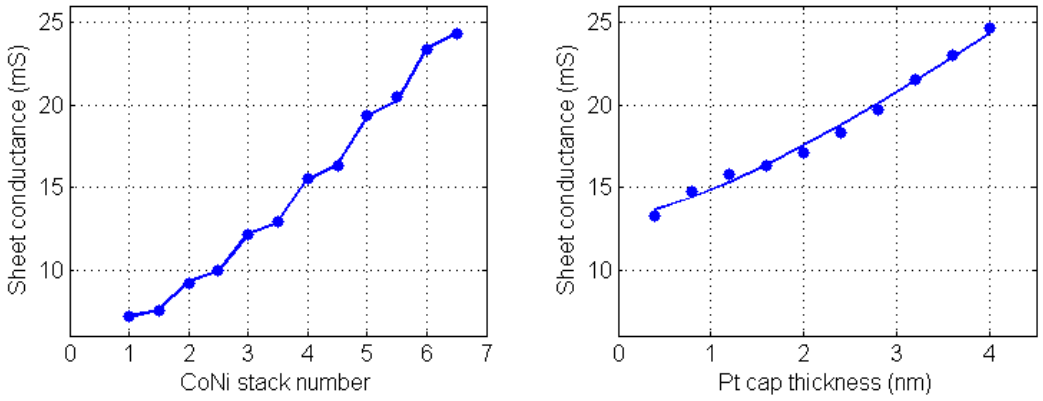

Figure 13: Sheet conductances as functions of CoNi stack number and Ptcap thickness obtained by CoNi-Pt model.

Table 3: Obtained parameters for CoNi-Pt model

	ρ_0 ($\mu\Omega$ cm)	λ (nm)		Error (mS^2)	1.27
TaUL	199.6	4.5		RMS (mS)	0.24
PtUL	141.3	2.6		T	0.95
Co	11.1	52.7		T_{TaPtUL}	0.07
Ni	8.1	23.2		T_{CoPtUL}	0.00
Ptcap	20.0	10.0		T_{CoPtcap}	0.02
Tacap	157.3	2.3		T_{TaPtcap}	1.00

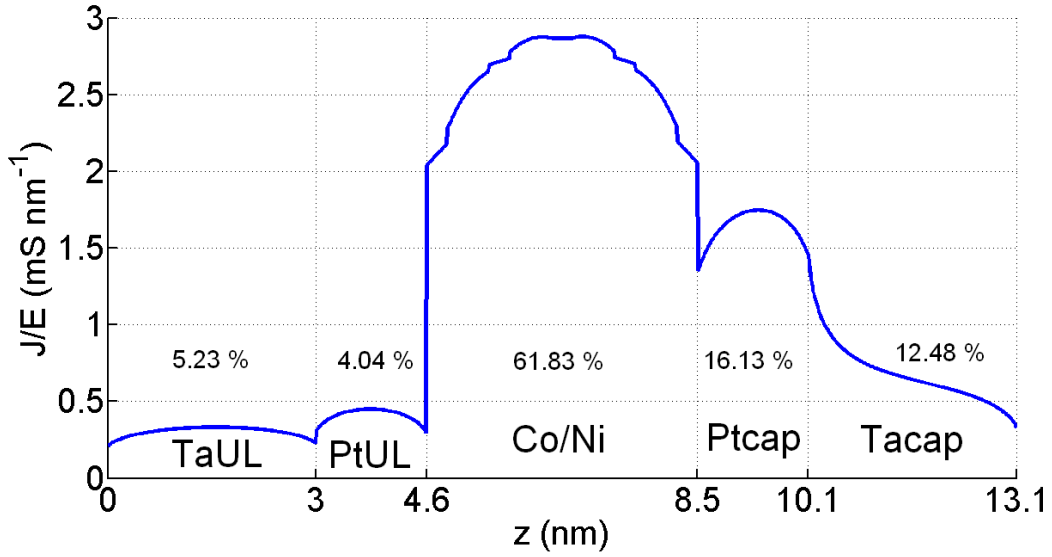

Figure 14: Current profile for CoNi-Pt model.

For both dependences, we obtained almost perfect fit. For Co/Ni layers we get again large mean free paths, but as can be seen in Fig. 14 (current profile), they tend to act as a single layer. The only boundary to be reached is the mean free path of top Pt, which we do not fully understand. Another slightly disturbing fact is the high transmission between top Pt and Ta that indicates a perfect interface between the two, which is highly improbable. However, if we let free the bulk constraint

for top Pt (the product was fixed at 200 in the fitting), then the product decreases to approximately 180 (indicating a high quality Pt layer), and the transmission between top Pt and Ta vanishes. For this case, we present only the current profile (Fig. 15), the total error does not change. In these cases, there is more current flowing through the top Pt compared to the bottom one, which is pleasing as the top Pt is supposed to be the better one. But to get such a result, we had to admit a thickness dependence of the bulk coefficients of the bottom Pt, which is not describable by our model, thus to exclude its dependence from the fitting.

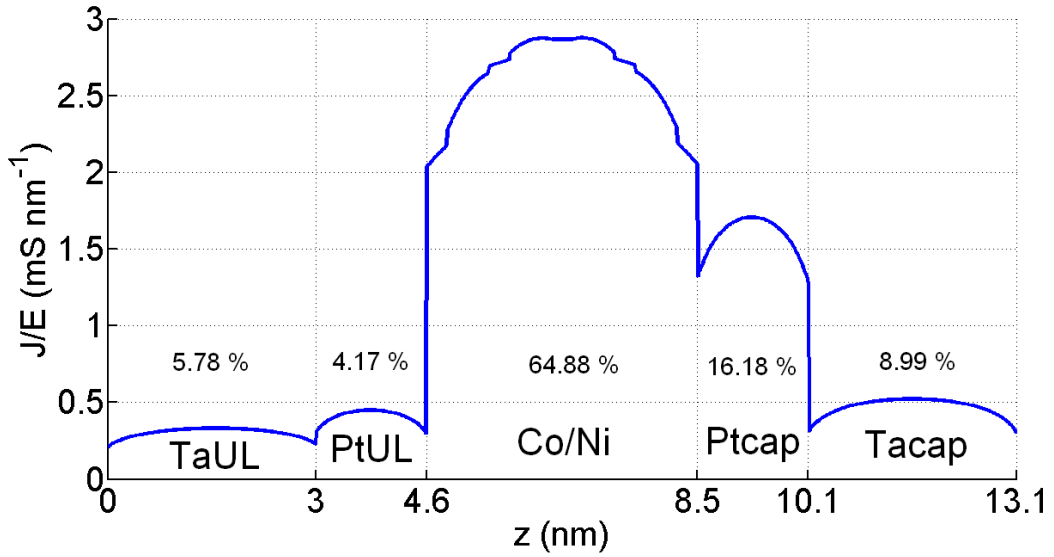

Figure 15: Current profile for CoNi-Pt model with lowered $\rho_0\lambda$ product for Ptcap layer.

6.3 CoNi-Pt-Ta model

Now we fit Co/Ni, Ptcap and Tacap dependences.At the beginning we excluded the Ta thickness dependences from our fitting, because their measured values do not indicate a typical Fuchs-Sondheimer behaviour. We will now try to include the top Ta dependence. Several parameters reach their upper boundaries during optimization, namely both Ta mean free paths are limited to 5 nm and top Pt mean free path to 10 nm. The results are shown in Fig. 16, Tab. 4 and Fig. 17.

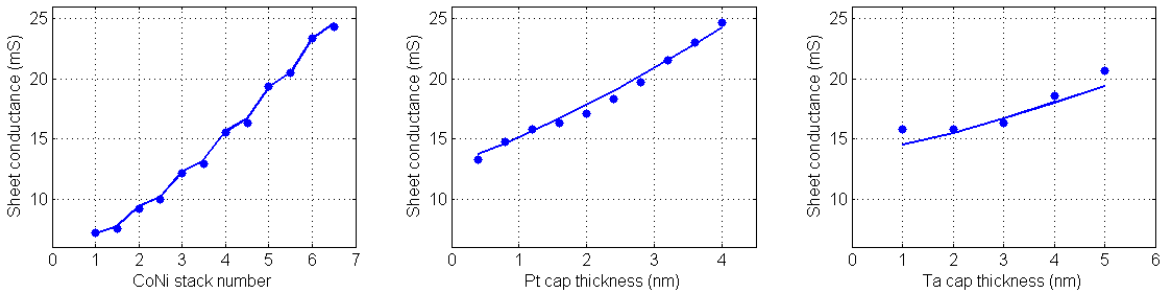

Figure 16: All the dependences (on CoNi stack number, Ptcap and Tacap thicknesses) obtained by CoNi-Pt-Ta model

Table 4: Obtained parameters for CoNi-Pt-Ta model

	ρ_0 ($\mu\Omega$ cm)	λ (nm)		Error (mS^2)	6.04
TaUL	298.0	5.0		RMS (mS)	0.47
PtUL	188.9	2.1		T	0.96
Co	8.0	46.0		T_{TaPtUL}	0.00
Ni	8.6	33.1		T_{CoPtUL}	0.00
Ptcap	21.9	10.0		T_{CoPtcap}	0.39
Tacap	62.7	5.0		T_{TaPtcap}	0.00

The theoretical curve for top Ta thickness dependence differs distinctly from the measured values and is the source of the error. This indicates the thickness depen-

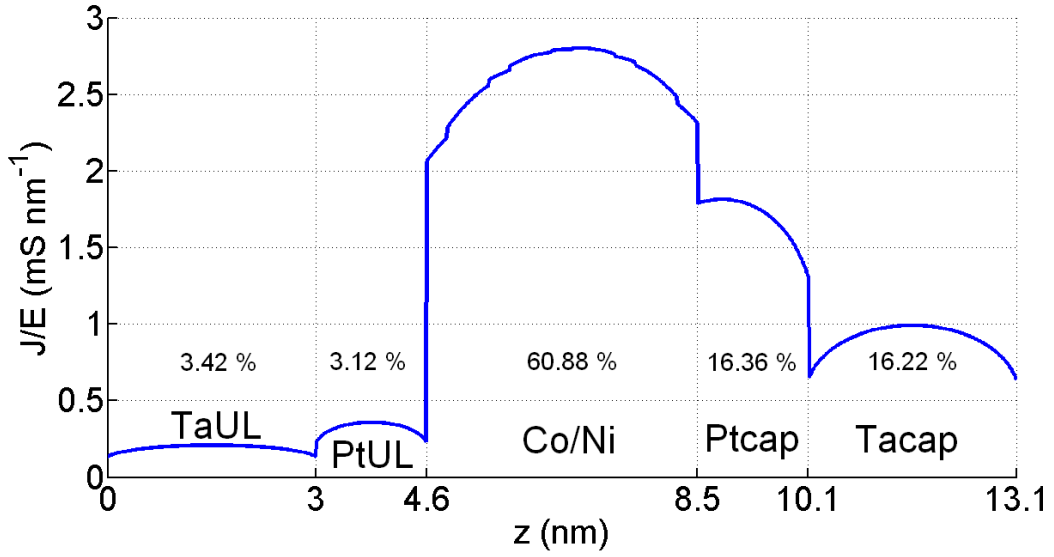

Figure 17: Current profile for CoNi-Pt-Ta model

dence of the bulk parameters also for top Ta, which is supposed to be the better one. The higher slope of the theoretical curve (originated by measured strong dependence of the total conductance of the sample on top Ta thickness and the effort to fit that with a constant parameters) also gives rise to a lot more current flowing through the layer.

7 Conclusions

Using the Fuchs-Sondheimer model, we were fitting experimental results of multilayer sample Ta/Pt/[Co/Ni]/Pt/Ta. In each series of the experiment, the thickness of only one layer was changing and the sheet resistances of the multilayer were measured. Therefore, five series of samples were fabricated and their sheet resistance was measured. Our initial goal was to fit all the experimental data with a single set of parameters (thickness independent). However, this was not reached, as the thickness dependence of certain parameters became unavoidable. For those materials (bottom and top Ta, bottom Pt) some structural change occurs as thickness increases. On the other hand, even from the reduced sets of measured results, we can present some conclusions.

All the presented current profiles indicate that Co/Ni multilayer acts as a single layer, therefore there is probably a lot of mixing between the two materials. In order to preserve the expected current distribution (more current flows through the top Pt than through the bottom Pt), we had to admit the thickness dependent bulk parameters also for bottom Pt. The following fitting resulted to a high quality top Pt layer (with a low $\rho_0\lambda$ product).

The problem of the Fuchs-Sondheimer theory is a large number of parameters, which are also strongly correlated (due to the transmission coefficients). Thus the function to be optimized does not have a single sharp minimum, but varies slowly with the variation of particular parameters. Changing initial values is not a problem, the fit indeed ends up in the same point, but changing particular parameters by non-small amount can result in a negligible change in the overall error (much smaller change that is the precision of the experiment), making it very difficult to determine the parameters precisely. It is pleasing though that the current profile also seems to change negligibly, making it a conceivable way of presenting the results (rather than the actual parameters). However, we can not claim that it is a general feature or if it happens only in certain cases. We do also keep in mind that before we had

started our analysis, we corrected all the results by a small amount. To increase the precision of the parameters, additional information of the sample is needed (in order to fix some parameters).

8 Appendix A: y parameter and measurement results

In this section we present the whole set of measured values for all the samples. Each sample was measured five times and their average was computed. The nominal sample (sub/Ta(3)/Pt(1.6)/[Co(0.3)/Ni(0.6)]4.5/Pt(1.6)/Ta(3)) was fabricated five times and its values are marked in the following table. All the measured values have been corrected so that all the nominal samples have the same value of sheet resistance.

In sec. 4 the parameter $y_{\mathrm{AB}} = \frac{m_{\mathrm{A}}\tau_{\mathrm{B}}}{m_{\mathrm{B}}\tau_{\mathrm{A}}}$ is introduced and we use in our calculations $y_{\mathrm{AB}} = \sigma_{0\mathrm{B}}/\sigma_{0\mathrm{A}}$. Plugging for the conductivities from Eq. 4.14 for two materials A and B, we get:

$$y_{\mathrm{AB}} = \frac{\sigma_{0\mathrm{B}}}{\sigma_{0\mathrm{A}}} = \frac{n_{\mathrm{B}}}{n_{\mathrm{A}}}\frac{m_{\mathrm{A}}\tau_{\mathrm{B}}}{m_{\mathrm{B}}\tau_{\mathrm{A}}} \tag{8.1}$$

Therefore, we are assuming that all the materials have equal electron density.

We could make a different choice for y_{AB}, using the mean free paths instead, $y_{\mathrm{AB}} = \lambda_{\mathrm{B}}/\lambda_{\mathrm{A}}$. Plugging for the mean free paths from Eq. 6.2 results in:

$$y_{\mathrm{AB}} = \frac{\lambda_{\mathrm{B}}}{\lambda_{\mathrm{A}}} = \frac{v_{F\mathrm{B}}\tau_{\mathrm{B}}}{v_{F\mathrm{A}}\tau_{\mathrm{A}}} \tag{8.2}$$

So in this case, we would assume equal Fermi velocities and effective electron masses for all materials. However, redefining the y parameter in our calculations, so that it obeys Eq. 8.2, leads to a negligible change in the results.

Table of measured results:

		measurement results (Ohm/square)						
	nm	1st	2nd	3rd	4th	5th	average	corrected values
CoNi stacking number	6.5	39	39.15	39.18	39.24	39.52	39.218	41.2
	6	40.73	40.77	40.84	40.74	40.84	40.784	42.8
	5.5	46.42	46.54	46.66	46.55	46.54	46.542	48.9
	5	49.41	49.33	49.4	49.31	49.32	49.354	51.8
	4.5	58.03	58.09	58.06	58.17	58.88	58.246	61.2
	4	61.42	61.28	61.23	60.93	61.09	61.19	64.3
	3.5	73.39	73.6	73.29	73.59	73.68	73.51	77.2
	3	78.36	78.47	78.3	78.4	78.23	78.352	82.3
	2.5	95.66	95.48	96.12	95.33	96.05	95.728	100.5
	2	104.71	103.97	104.38	103.89	104.22	104.234	109.5
	1.5	126.4	126.55	126.05	126.45	125.75	126.24	132.6
	1	132.28	132.1	131.97	132.11	132.11	132.114	138.8
Pt cap thickness	0.4	73.81	73.45	73.49	73.51	73.12	73.476	75.4
	0.8	66.02	66.27	66	66	66.22	66.102	67.8
	1.2	61.8	61.7	61.52	61.57	61.55	61.628	63.2
	1.6	59.63	59.42	59.7	59.72	59.59	59.612	61.2
	2	56.92	56.96	57.06	56.96	56.89	56.958	58.5
	2.4	53.47	53.34	53.27	53.4	53.25	53.346	54.7
	2.8	49.45	49.41	49.2	49.37	49.38	49.362	50.7
	3.2	45.22	45.17	45.28	45.13	45.22	45.204	46.4
	3.6	42.4	42.21	42.49	42.32	42.33	42.35	43.5
	4	39.58	39.43	39.45	39.61	39.44	39.502	40.5
Ta cap thick.	1	65.82	65.68	65.72	65.78	65.72	65.744	63.5
	2	65.76	65.5	65.36	65.44	65.61	65.534	63.3
	3	63.19	63.28	63.35	63.45	63.29	63.312	61.2
	4	55.94	55.42	55.6	55.68	55.66	55.66	53.8
	5	50	49.91	50.19	50.32	50.06	50.096	48.4
Pt UL thickness	0.4	78.44	78.37	78.1	78.42	78.04	78.274	79.2
	0.8	72.5	72.85	72.82	73	72.92	72.818	73.7
	1.2	67.5	67.66	67.65	67.34	67.48	67.526	68.4
	1.6	60.44	60.43	60.53	60.35	60.41	60.432	61.2
	2	56.32	56.35	56.49	56.51	56.61	56.456	57.1
	2.4	53.19	53.43	53.52	53.37	53.27	53.356	54
	2.8	50.36	50.33	50.39	50.63	50.41	50.424	51
	3.2	48.1	48.17	47.85	48.05	48.01	48.036	48.6
	3.6	45.23	45.24	45.25	45.42	45.2	45.268	45.8
	4	42.76	42.84	42.94	42.72	42.82	42.816	43.3
Ta UL thick.	1	74.86	74.81	74.88	74.71	74.15	74.682	71.1
	2	70.29	70.3	70.13	70.04	69.94	70.14	66.8
	3	64.08	64	63.79	64.13	65.34	64.268	61.2
	4	60.04	60	59.83	59.95	59.62	59.888	57
	5	55.4	55.48	55.31	55.39	57.1	55.736	53.1

9 Appendix B: boundary conditions for two layers

Assume a bilayer system sketched on Fig. 18. Layer A (B) is described by its bulk conductivity $\sigma_{0\mathrm{A}}$ ($\sigma_{0\mathrm{B}}$) and electron mean free path λ_{A} (λ_{B}). The relaxation time τ_{A} (τ_{B}) and electron effective mass m_{A} (m_{B}) will be hidden in the y parameter. We can solve the Boltzmann transport equation in each layer to obtain the solution for the distribution function $g_{\pm}$ (Eq. 4.3). Afterwards, we apply the boundary conditions to determine $F_{\pm}$. The outer interfaces are described by the Fuchs specularity factors (p_{A} at $z = 0$ and p_{B} at $z = b$). The inner interface ($z = a$) is described by reflection R and transmission T coefficient.

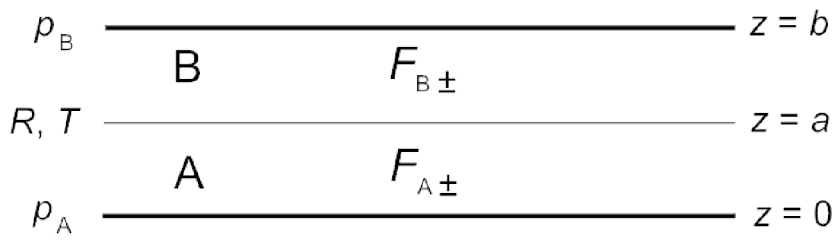

Figure 18: A schematic of a bilayer system. The outer interfaces are described by the Fuchs specularity coefficients and the inner interface by specular reflection and transmission coefficients.

The boundary conditions can be written as follows:

$$g_{\mathrm{A}+} = p_{\mathrm{A}} g_{\mathrm{A}-}, \qquad \text{at } z = 0 \tag{9.1}$$

$$g_{\mathrm{A}-} = R g_{\mathrm{A}+} + T g_{\mathrm{B}-}, \qquad \text{at } z = a \tag{9.2}$$

$$g_{\mathrm{B}+} = R g_{\mathrm{B}-} + T g_{\mathrm{A}+}, \qquad \text{at } z = a \tag{9.3}$$

$$g_{\mathrm{B}-} = p_{\mathrm{B}} g_{\mathrm{B}+}, \qquad \text{at } z = b \tag{9.4}$$

We plug in for $g_{\pm}$, $y_{\mathrm{AB}} = \frac{m_{\mathrm{A}}\tau_{\mathrm{B}}}{m_{\mathrm{B}}\tau_{\mathrm{A}}}$ to get the final matrix equation:

$$\mathbf{M} = \begin{pmatrix} 1 & -p_{\mathrm{A}} & 0 & 0 \\ -R\exp\left(-\frac{a}{\lambda_{\mathrm{A}}\cos\beta}\right) & \exp\left(\frac{a}{\lambda_{\mathrm{A}}\cos\beta}\right) & 0 & -Ty_{\mathrm{AB}}\exp\left(\frac{a}{\lambda_{\mathrm{B}}\cos\beta}\right) \\ -T\exp\left(-\frac{a}{\lambda_{\mathrm{A}}\cos\beta}\right) & 0 & y_{\mathrm{AB}}\exp\left(-\frac{a}{\lambda_{\mathrm{B}}\cos\beta}\right) & -Ry_{\mathrm{AB}}\exp\left(\frac{a}{\lambda_{\mathrm{B}}\cos\beta}\right) \\ 0 & 0 & -p_{\mathrm{B}}\exp\left(-\frac{b}{\lambda_{\mathrm{B}}\cos\beta}\right) & \exp\left(\frac{b}{\lambda_{\mathrm{B}}\cos\beta}\right) \end{pmatrix}$$

$$\mathbf{M}\begin{bmatrix} F_{\mathrm{A}+} \\ F_{\mathrm{A}-} \\ F_{\mathrm{B}+} \\ F_{\mathrm{B}-} \end{bmatrix} = \begin{bmatrix} p_{\mathrm{A}} - 1 \\ R + Ty_{\mathrm{AB}} - 1 \\ y_{\mathrm{AB}}R + T - y_{\mathrm{AB}} \\ p_{\mathrm{B}} - 1 \end{bmatrix}$$

Extension for an arbitrary number of layers is straightforward. For example, in the case of three conducting layers, the size of the matrix $\mathbf{M}$ will be 6×6.

The integration in Eqs. 4.17, 4.18 (to compute the total conductivity of the multilayer and the current distribution) is performed over β, therefore in every integration step, we solve this matrix equation to obtain $F_{\pm}$. For small systems (consisting of only a few layers), it is easier to solve the matrix equation analytically to obtain explicit expressions for $F_{\pm}(\beta)$. This speeds up the whole procedure, because we do not have to solve the matrix equation in every integration step. However, for large systems (even for only 5 layers), the expressions become too complicated, that it is no longer advantageous.

10 Appendix C: the correction of measured values

The experiment involved measurements of five series of samples, in each series only the thickness of one layer was changing (or the Co/Ni stack number). Thus the nominal sample (Fig. 5) was made five times. Each sample was measured five times and their average was computed. It is expectable that all the five nominal samples should have the same value of resistance, but small deviations occur. This can be caused by the fact that all the nominal samples were prepared in different times and in slightly different conditions, thus they slightly differ from each other.

For the fitting procedure to be easier, we decided to correct all the measurement results, so that all values of the nominal sample are the same. We simply took the average of all five resistances of the nominal sample and then multiply each series by a factor such that the resistance value of the nominal sample ends up being the computed average. The corrected values we used for the fitting. It is now natural to ask, how it influences the results of the fitting.

In each fitting, we were minimizing the sum of the squares of differences of computed and measured values (called error) or equivalently the root mean square (RMS). Had not we corrected the values, it is expectable that we would obtain very similar results, if we were fitting all the series at once. If we now consider only the values of the nominal samples, then by minimizing the error, we would end up with a resistance value very close to the average. So performing the fit with original and corrected values, we would get almost the same result (as long as we fit all the series at once), only the error would be higher for the original values.

Some changes would occur, if we were fitting only some of the series. Then the fit based on the original values would be close to the fit based on the corrected ones only if we were considering the average of only the values of the series involved. If we look closely on the measured results, we can see that the values of the nominal samples substantially differ in the series involving the Ta thickness changing (though there is no reason for that to be so). In sec. 6.1 we excluded the Ta series

from the fitting so there would be some change in the result if we used the original values compared to the corrected ones. However, as we found no reason for that (for the change in Ta series), it seems to be caused by the limitation in the accuracy of the experiment and we would not get any new information by doing it this way.

11 References

[1] Wikipedia, Stoner model of ferromagnetism, (2014).

[2] P. M. Haney, H.-W. Lee, K.-J. Lee, A. Manchon, and M. D. Stiles, *Current induced torques and interfacial spin-orbit coupling: Semiclassical modeling*, Phys. Rev. B **87**, 174411 (2013).

[3] S. Maekawa, Current-induced domain wall motion, (2014).

[4] A. Brataas, *Spintronics: Chiral domain walls move faster*, Nature Nanotechnology **8**, 485 (2013).

[5] F. J. Jedema, H. B. Heersche, A. T. Filip, J. J. A. Baselmans, and B. J. van Wees, *Electrical detection of spin precession in a metallic mesoscopic spin valve*, Nature **416**, 713 (2002).

[6] N. Poli, *Spin transport in normal and superconducting nanowires*, Ph.D. thesis, Albanova University Center, 2007.

[7] W. Thomson, Proc. R. Soc. **8**, 546 (1857).

[8] M. N. Baibich, J. M. Broto, A. Fert, F. N. Van Dau, F. Petroff, P. Etienne, G. Creuzet, A. Friederich, and J. Chazelas, *Giant Magnetoresistance of (001)Fe/(001)Cr Magnetic Superlattices*, Phys. Rev. Lett. **61**, 2472 (1988).

[9] G. Binasch, P. Grünberg, F. Saurenbach, and W. Zinn, *Enhanced magnetoresistance in layered magnetic structures with antiferromagnetic interlayer exchange*, Phys. Rev. B **39**, 4828 (1989).

[10] M. Julliere, *Tunneling between ferromagnetic films*, Physics Letters A **54**, 225 (1975).

[11] H. Yu, *Thermal spin transfer torque and transverse spin relaxation in spin valves*, Ph.D. thesis, École Polytechnique Fédérale de Lausanne, 2011.

[12] A. G. Aronov and G. E. Pikus, *Spin injection into semiconductors*, Sov. Phys. Semicond. **10**, 698 (1976).

[13] Y. Tserkovnyak, A. Brataas, and G. E. W. Bauer, *Enhanced Gilbert Damping in Thin Ferromagnetic Films*, Phys. Rev. Lett. **88**, 117601 (2002).

[14] M. Dyakonov and V. Perel, *Current-induced spin orientation of electrons in semiconductors*, Physics Letters A **35**, 459 (1971).

[15] N. Mott, *The electrical conductivity of transition metals*, Proc. R. Soc. Lond. A **153**, 699 (1936).

[16] A. V. Khvalkovskiy, V. Cros, D. Apalkov, V. Nikitin, M. Krounbi, K. A. Zvezdin, A. Anane, J. Grollier, and A. Fert, *Matching domain-wall configuration and spin-orbit torques for efficient domain-wall motion*, Physical Review B **87**, 020402 (2013).

[17] T. Jungwirth, J. Wunderlich, and K. Olejník, *Spin Hall effect devices*, Nature Materials **11**, 382 (2012).

[18] J. E. Hirsch, *Spin Hall Effect*, Phys. Rev. Lett. **83**, 1834 (1999).

[19] S. Zhang, *Spin Hall Effect in the Presence of Spin Diffusion*, Phys. Rev. Lett. **85**, 393 (2000).

[20] Y. K. Kato, R. C. Myers, A. C. Gossard, and D. D. Awschalom, *Observation of the Spin Hall Effect in Semiconductors*, Science **306**, 1910 (2004).

[21] J. Wunderlich, B. Kaestner, J. Sinova, and T. Jungwirth, *Experimental Observation of the Spin-Hall Effect in a Two-Dimensional Spin-Orbit Coupled Semiconductor System*, Phys. Rev. Lett. **94**, 047204 (2005).

[22] J. Slonczewski, *Current-driven excitation of magnetic multilayers*, Journal of Magnetism and Magnetic Materials **159**, L1 (1996).

[23] L. Liu, C. F. Pai, Y. Li, H. W. Tseng, D. C. Ralph, and R. A. Buhrman, *Spin torque switching with the giant spin Hall effect of tantalum*, Science **336**, 555 (2012).

[24] L. Liu, T. Moriyama, D. C. Ralph, and R. A. Buhrman, *Spin-Torque Ferromagnetic Resonance Induced by the Spin Hall Effect*, Phys. Rev. Lett. **106**, 036601 (2011).

[25] L. Liu, O. J. Lee, T. J. Gudmundsen, D. C. Ralph, and R. A. Buhrman, *Current-Induced Switching of Perpendicularly Magnetized Magnetic Layers Using Spin Torque from the Spin Hall Effect*, Physical Review Letters **109**, 096602 (2012).

[26] L. Liu, R. A. Buhrman, and D. C. Ralph, *Review and Analysis of Measurements of the Spin Hall Effect in Platinum*, ArXiv e-prints (2011).

[27] C.-F. Pai, L. Liu, Y. Li, H. W. Tseng, D. C. Ralph, and R. A. Buhrman, *Spin transfer torque devices utilizing the giant spin Hall effect of tungsten*, Applied Physics Letters **101**, (2012).

[28] I. M. Miron, G. Gaudin, S. Auffret, B. Rodmacq, A. Schuhl, S. Pizzini, J. Vogel, and P. Gambardella, *Current-driven spin torque induced by the Rashba effect in a ferromagnetic metal layer*, Nature Materials **9**, 230 (2010).

[29] T. Emori, D. C. Bono, and G. S. D. Beach, *Interfacial current-induced torques in Pt/Co/GdOx*, Applied Physics Letters **101**, 042405 (2012).

[30] G. Malinowski, O. Boulle, and M. Kläui, *Current-induced domain wall motion in nanoscale ferromagnetic elements*, Journal of Physics D: Applied Physics **44**, 384005 (2011).

[31] J. Singh, *Modern Physics for Engineers* (Wiley-VCH Verlag GmbH & Co. KGaA, Weinheim, Germany, 2011).

[32] E. Sondheimer, *The mean free path of electrons in metals*, Advances in Physics **1**, 1 (1952).

[33] J. Barnaś, A. Fuss, R. E. Camley, P. Grünberg, and W. Zinn, *Novel magnetoresistance effect in layered magnetic structures: Theory and experiment*, Physical Review B **42**, 8110 (1990).

[34] M. H. Read and C. Altman, *A new structure in tantalum thin films*, Applied Physics Letters **7**, 51 (1965).

[35] H. Hoffmann and J. Vancea, *Critical assessment of thickness-dependent conductivity of thin metal films*, Thin Solid Films **85**, 147 (1981).